MEASUREMENT OF NEUTRINO FLUX FROM THE PRIMARY PROTON–PROTON FUSION PROCESS IN THE SUN WITH THE BOREXINO DETECTOR

O. Yu. Smirnov [1,*] *M. Agostini* [2], *S. Appel* [2], *G. Bellini* [3],
J. Benziger [4], *D. Bick* [5], *G. Bonfini* [6], *D. Bravo* [7], *B. Caccianiga* [3],
F. Calaprice [8], *A. Caminata* [9], *P. Cavalcante* [6], *A. Chepurnov* [10],
K. Choi [11], *D. D'Angelo* [3], *S. Davini* [12], *A. Derbin* [13],
L. Di Noto [9], *I. Drachnev* [12], *A. Empl* [14], *A. Etenko* [15],
K. Fomenko [1], *D. Franco* [16], *F. Gabriele* [6], *C. Galbiati* [8],
C. Ghiano [9], *M. Giammarchi* [3], *M. Goeger-Neff* [2], *A. Goretti* [8],
M. Gromov [10], *C. Hagner* [5], *E. Hungerford* [14], *Aldo Ianni* [6],
Andrea Ianni [8], *K. Jedrzejczak* [17], *M. Kaiser* [5], *V. Kobychev* [18],
D. Korablev [1], *G. Korga* [6], *D. Kryn* [16], *M. Laubenstein* [6],
B. Lehnert [19], *E. Litvinovich* [15, 20], *F. Lombardi* [6], *P. Lombardi* [3],
L. Ludhova [3], *G. Lukyanchenko* [15, 20], *I. Machulin* [15, 20], *S. Manecki* [7],
W. Maneschg [21], *S. Marcocci* [12], *E. Meroni* [3], *M. Meyer* [5],
L. Miramonti [3], *M. Misiaszek* [6, 17], *P. Mosteiro* [8], *V. Muratova* [13],
B. Neumair [2], *L. Oberauer* [2], *M. Obolensky* [16], *F. Ortica* [22],
K. Otis [23], *L. Pagani* [9], *M. Pallavicini* [9], *L. Papp* [2],
L. Perasso [9], *A. Pocar* [23], *G. Ranucci* [3], *A. Razeto* [6],
A. Re [3], *A. Romani* [22], *R. Roncin* [6, 16], *N. Rossi* [6],
S. Schönert [2], *D. Semenov* [13], *H. Simgen* [21], *M. Skorokhvatov* [15, 20],
A. Sotnikov [1], *S. Sukhotin* [15], *Yu. Suvorov* [15, 20], *R. Tartaglia* [6],
G. Testera [9], *J. Thurn* [19], *M. Toropova* [15], *E. Unzhakov* [13],
R. B. Vogelaar [7], *F. von Feilitzsch* [2], *H. Wang* [24], *S. Weinz* [25],
J. Winter [25], *M. Wojcik* [17], *M. Wurm* [25], *Z. Yokley* [7],
O. Zaimidoroga [1], *S. Zavatarelli* [9], *K. Zuber* [19], *G. Zuzel* [17]*
(The Borexino Collaboration)

[1] Joint Institute for Nuclear Research, Dubna
[2] Physics Department and Excellence Cluster "Universe",
Technische Universität München, Garching, Germany

---

*E-mail: osmirnov@jinr.ru

[3] Dipartimento di Fisica, Università degli Studi e INFN, Milano, Italy

[4] Chemical Engineering Department, Princeton University, Princeton, NJ, USA

[5] Institut für Experimentalphysik, Universität, Hamburg, Germany

[6] INFN Laboratori Nazionali del Gran Sasso, Assergi (AQ), Italy

[7] Physics Department, Virginia Polytechnic
Institute and State University, Blacksburg, VA, USA

[8] Physics Department, Princeton University, Princeton, NJ, USA

[9] Dipartimento di Fisica, Università degli Studi e INFN, Genova, Italy

[10] Skobeltsyn Institute of Nuclear Physics, Lomonosov Moscow State University, Moscow

[11] Department of Physics and Astronomy, University of Hawaii, Honolulu, HI, USA

[12] Gran Sasso Science Institute (INFN), L'Aquila, Italy

[13] St. Petersburg Nuclear Physics Institute National
Research Center "Kurchatov Institute", Gatchina, Russia

[14] Department of Physics, University of Houston, Houston, TX, USA

[15] National Research Center "Kurchatov Institute", Moscow

[16] AstroParticule et Cosmologie, Université Paris Diderot, CNRS/IN2P3,
CEA/IRFU, Observatoire de Paris, Sorbonne Paris Cité, Paris Cedex 13, France

[17] M. Smoluchowski Institute of Physics, Jagiellonian University, Krakow, Poland

[18] Kiev Institute for Nuclear Research, Kiev

[19] Department of Physics, Technische Universität Dresden, Dresden, Germany

[20] National Research Nuclear University MEPhI
(Moscow Engineering Physics Institute), Moscow

[21] Max-Planck-Institut für Kernphysik, Heidelberg, Germany

[22] Dipartimento di Chimica, Biologia e Biotecnologie, Università e INFN, Perugia, Italy

[23] Amherst Center for Fundamental Interactions and Physics Department,
University of Massachusetts, Amherst, MA, USA

[24] Physics and Astronomy Department, University of California Los Angeles (UCLA),
Los Angeles, California, USA

[25] Institute of Physics and Excellence Cluster PRISMA,
Johannes Gutenberg-Universität Mainz, Mainz, Germany

Neutrino produced in a chain of nuclear reactions in the Sun starting from the fusion of two protons for the first time has been detected in a real-time detector in spectrometric mode. The unique properties of the Borexino detector provided an opportunity to disentangle pp-neutrino spectrum from the background components. A comparison of the total neutrino flux from the Sun with solar luminosity in photons provides a test of the stability of the Sun on the 10^5 yr time scale and sets a strong limit on the power production in the unknown energy sources in the Sun of no more than 4% of the total energy production at 90% C.L.

PACS: 26.65.+t

INTRODUCTION

The solar photon luminosity (a total power radiated in the form of photons into space) is determined by measuring the total solar irradiance by spacecrafts over the wide subrange of the electromagnetic spectrum, from X-rays to radio

wavelengths; it has been accurately monitored for decades. The luminosity $L_\odot = 3.846 \cdot 10^{26}$ W is measured for a precision of 0.4% with the largest uncertainty of about 0.3% due to disagreements between the measurements of different satellite detectors [1,2]. The energy lost by neutrinos adds $L_\nu = 0.023 L_\odot$ to this value [3]. The solar luminosity constraint on the solar neutrino fluxes can be written as [4]

$$\frac{L_\odot}{4\pi(1\,\text{a.u.})^2} = \sum \alpha_i \Phi_i, \tag{1}$$

where 1 a.u. is the average Earth–Sun distance, the coefficient α_i is the amount of energy provided to the star by nuclear fusion reactions associated with each of the important solar neutrino fluxes, Φ_i. The numerical values of the α's are determined to an accuracy of 10^{-4} and better.

The estimated uncertainty in the luminosity of the Sun corresponds to less than 3% uncertainty in total solar neutrino flux.

The Sun is a weakly variable star, its luminosity has short-term fluctuations [2,5]. The major fluctuation occurs during the eleven-year solar cycle with an amplitude of about 0.1%. Long-term solar variability (such as the Maunder minimum in the 16th and 17th centuries) is commonly believed to be less than the short-term variations.

Because of the relation (1) between the solar photon and neutrino luminosity, the measurement of the total neutrino luminosity will provide a test of the stability of the Sun at the time scale of 40000 yr [6], the time needed for the radiation born at the center of the Sun to arrive to its surface. Finding a disagreement between $L_\odot$ and L_ν would have significant long-term enviromental implications, and in the case of an agreement of two measurements it would be possible to limit the unknown sources of the solar energy, different from the known thermonuclear fusion of light elements in the pp-chain and CNO-cycle.

The main neutrino sources in the Sun are the pp- and ^{7}Be reactions, providing roughly 91 and 7% of the total neutrino flux, respectively. Borexino already measured ^{7}Be neutrino flux with 5% precision [7], but till recent time the pp-neutrino flux was derived in a differential measurement using the data of solar detectors.

Solar pp-neutrino measurement is a critical test of stellar evolution theory, discussion of the physics potential of the pp solar neutrino flux measurement can be found in [8–10] (at the moment of the discussion the parameters space for MSW solution were not established yet, thus the authors gave priority to this part of the physical potential).

A number of projects aiming to perform pp-neutrino detection have been put forward in past two decades, but with all the time passed since the proposals, none of them started the operation facing the technical problems with realization. The principal characteristics of the proposals are presented in Table 1. The

Table 1. Key characteristics of the solar neutrino projects sensitive to the *pp*-neutrino. The number of expected neutrino is calculated for the fraction of the neutrino spectrum above the threshold, but the region of sensitivity (limited, i.e., by signals-to-backgrounds ratio of 1) could be stricter

Project, reference	Method	Threshold, keV	Resolution	Mass, t	Reaction	*pp* events, d^{-1}
LENS [13]	^{176}Yb, LS	$301(\nu)$	7% @1 MeV	20 (8% nat. ^{176}Yb)	$^{176}\text{Yb}+\nu_e \rightarrow$ $^{176}\text{Lu}+e^-$	0.5
INDIUM [14]	^{115}In LS	$118(\nu)$	5–10% @1 MeV	4	$^{115}\text{In}+\nu_e \rightarrow$ $^{115}\text{Sn}^*(613)+e^-$	1.0
GENIUS [15]	^{76}Ge scatt.	$11(e^-)$ $59(\nu)$	0.3% @300 keV	1 10	$\nu+e^- \rightarrow \nu+e^-$	1.8 18
HERON [16,17]	Superfluid ^{4}He protons/phonons + uv	$50(e^-)$ $141(\nu)$	8.3% @364 keV	10	$\nu+e^- \rightarrow \nu+e^-$	14
XMASS [18]	Liquid Xe scintill.	$50(e^-)$ $141(\nu)$	17.5% @100 keV	10	$\nu+e^- \rightarrow \nu+e^-$	14
CLEAN [19]	Liquid Ne	$20(e^-)$ $82(\nu)$		135	$\nu+e^- \rightarrow \nu+e^-$	7.2
HELLAZ [20]	He (5 atm), TPC	$100(e^-)$ $217(\nu)$	6% @800 keV	2000 m^3	$\nu+e^- \rightarrow \nu+e^-$	7
MOON [21]	Drift chambers	$168(\nu)$	12.4% FWHH @1 MeV	3.3	$\nu_e+^{100}\text{Mo} \rightarrow$ $^{100}\text{Tc}+e^-$	1.1
MUNU [22]	TPC, CF$_4$ direction	$100(e^-)$ $217(\nu)$	16% FWHH @1 MeV	0.74 (200 m^3)	$\nu+e^- \rightarrow \nu+e^-$	0.5
NEON [23]	He, Ne scintill.	$20(e^-)$ $82(\nu)$	16% FWHH @100 keV	10	$\nu+e^- \rightarrow \nu+e^-$	18
10 t LS [24,25]	LS	$170(e^-)$ $310(\nu)$	10.5 keV @200 keV	10	$\nu+e^- \rightarrow \nu+e^-$	1.8
Borexino [26]	LS	$165(e^-)$ $305(\nu)$	5% @1 MeV	75.5 (fiducial)	$\nu+e^- \rightarrow \nu+e^-$	13.6

radiochemical experiments sensitive to the solar pp-neutrinos (SAGE [11] and GALLEX [12]) are not cited in the table, the combined best fit of the radiochemical and other solar experiments gives solar pp-neutrino flux of $(6.0 \pm 0.8) \cdot 10^{10}$ cm$^{-2} \cdot$ s^{-1} [11] in a good agreement with expected value of $6.0 \cdot (1.000 \pm 0.006) \cdot 10^{10}$ cm$^{-2} \cdot$ s^{-1}.

A possibility to use ultrapure liquid organic scintillator as a low-energy solar neutrino detector for was for the first time discussed in [24, 25]. The authors come to the conclusion that a liquid scintillator detector with an active volume of 10 t is a feasible tool to register the solar pp-neutrino if operated at the target level of radiopurity for Borexino and good energy resolution (5% at 200 keV) is achieved.

1. BOREXINO DETECTOR

The Borexino detector has a dome-like structure (see Fig. 1), 16 m in diameter, filled with a mass of 2,400 t of highly purified water which acts as the shield against the external radioactive emissions of the rocks and the environment that surrounds the facility. The water buffer acts also as an effective detector of residual cosmic rays. Within the volume of water a steel sphere is mounted which hosts 2,200 looking inward photomultiplier tubes providing 34% geometrical coverage. On the outer side of the stainless sphere 200 PMTs of the outer muon veto detector are mounted, these PMTs detect the Cherenkov light caused by muons passing through.

The sphere contains one thousand tonnes of pseudocumene. Finally, the innermost core of the facility contains roughly 280 t of the scintillating liquid bounded within a 100-μm-thick nylon transparent bag with ~ 4.2 m radius. The water and the pseudocumene buffers, as well as the scintillator itself, have a record-low level of radioactive purity. The energy of each event is measured using light response of the scintillator, and the position of the interaction is
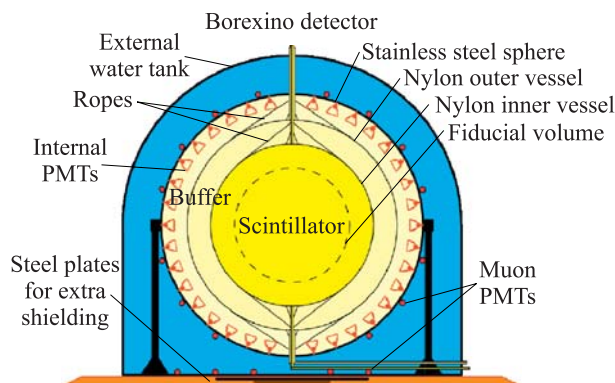
Fig. 1. Schematic view of the Borexino detector

determined using timing information from the PMTs. The latter is important for the selection of the innermost cleanest part of the detector within 3 m radius, as only the internal 100 t of scintillator have the radioactive background low enough to allow the solar neutrino detection; the scintillator layer close to the nylon serves as an active shield against the γ originating from the nylon trace radioactive contamination. The threshold of the detector is set as low as possible to exclude triggering from the random dark count of PMTs. The Borexino has an excellent energy resolution for its size, this is the result of the high light yield of ~ 500 p.e./MeV/2000 PMTs. The energy resolution is as low as 5% at 1 MeV.

2. DATA PROCESSING

The low-energy range, namely 165–590 keV, of the Borexino experimental spectrum has been recently carefully analyzed with a purpose of the *pp*-neutrino flux measurement [27]. The data were acquired from January 2012 to May 2013 and correspond to 408 live days of data taking. These data were collected at the beginning of the second phase of Borexino which had started after the additional purification of the liquid scintillator following the calibration campaign of 2010–2011 [28]. The main backgrounds for the solar neutrino studies were significantly reduced in Phase 2, the content of ^{85}Kr is compatible with zero, and background from ^{210}Bi reduced by a factor of 3 to 4 compared to the values observed at the end of Phase 1 just before the purification.

The experimental spectrum is presented in Fig. 2. The main features of the experimental spectrum can be seen in the figure: the main contribution comes from ^{14}C decays at low energies (below 200 keV), the monoenergetic peak corresponds to 5.3 MeV α-particles from ^{210}Po decay. The statistics in the first bins used in the analysis is very high, of the order of $5 \cdot 10^5$ events, demanding development of the very precise model for the studies — the allowed systematic precision at low-energy part should be comparable with the statistical fluctuations of 0.14%.

2.1. Data Analysis. The Borexino spectrum in the low-energy range is composed mainly of the events from β decays of ^{14}C present in liquid organic oscillator in trace quantities, its measured abundance with respect to ^{12}C is $(2.7 \pm 0.1) \cdot 10^{-18}$ g/g. The β decay of ^{14}C is an allowed ground-state to ground-state $(0^+ \rightarrow 1^+)$ Gamow–Teller transition with an endpoint energy $E_0 = (156.476 \pm 0.004)$ keV.

In Borexino the amount of the active PMTs is high (~ 2000), demanding setting of the high acquisition threshold in order to exclude detector triggering from random coincidence of dark count in PMTs: hardware trigger was set at the level of 25 PMTs in coincidence within 30-ns window, providing negligible random events count. The acquisition efficiency corresponding to 25 triggered
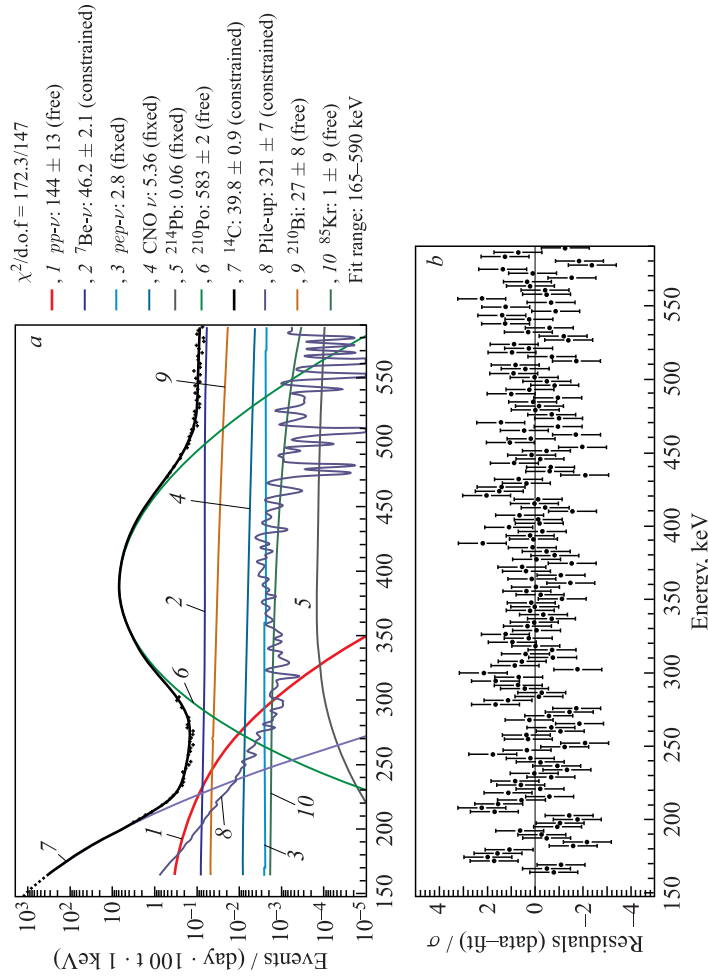
Fig. 2 (color online). Borexino energy spectrum between 165 and 590 keV. The *pp*-neutrino component is shown in red (*1*), the ^{14}C spectrum in dark purple (*7*), and the synthetic pile-up in light purple (*8*). The large green peak is ^{210}Po α decays (*6*). ^{7}Be (dark blue, (*2*)), *pep* (*3*) and CNO (light blue (*4*)) solar neutrinos, and ^{210}Bi (orange (*9*)) spectra are almost flat in this energy region

PMTs is roughly 50% and corresponds to the energy release of ~ 50 keV. In present analysis, the same as in the "pp" analysis, the threshold was set at the lowest possible value at ~ 60 triggered PMTs (~ 160 keV). In independent measurement with laser the trigger inefficiency was found to be below 10^{-5} for energies above 120 keV [26].

2.2. Energy Resolution.   The most sensitive part of the analysis is the behavior of the energy resolution with energy. The variance of the signal is smeared by the dark noise of the detector (composed of the dark noise from individual PMTs). In order to account for the dark noise, the data were sampled every two seconds forcing randomly the fired triggers. Some additional smearing of the signal is expected because of the continuously decreasing number of PMTs in operation. The amount of live PMTs is followed in real time and we know precisely its distribution, so in principle this additional smearing can be precisely accounted for. It was found that the following approximation works well in the energy region of interest:

$$\sigma_N^2 = N(p_0 - p_1 v_1) + N^2(v_T(N) + v_f),$$

where $N = N_0 \langle f(t) \rangle_T$ is an average number of working PMTs during the period of the data taking; $f(t)$ is a function describing the amount of working PMTs in time with $f(0) = N_0$. The last parameter here is $v_f(N) = \langle f^2(t) \rangle_T - \langle f(t) \rangle_T^2$, it is the variance of the $f(t)$ function over the time period of the data taking.

An additional contribution to the variance of the signal was identified, it is the intrinsic width of the scintillation response. From the simple consideration this contribution reflects the additional variations due to the fluctuations of the delta electrons production and the energy scale nonlinearity. It should scale inversely proportional to the energy loss. Because of the limited range of the sensitivity to this contribution, basically restricted to the very tail of the ^{14}C spectrum, the precise energy dependence could be neglected and we used a constant additional term in the resolution. Taking it all together, the variance of the energy resolution (in terms of the used energy estimator) is

$$\sigma_N^2 = N(p_0 - p_1 v_1) + N^2(v_T(N) + v_f) + \sigma_d^2 + \sigma_{\text{int}}^2,$$

where σ_d is a contribution of the dark noise (fixed) and σ_{int} is a contribution from the intrinsic line shape smearing. The probability p_1 is linked to the energy estimator with relation $n = N p_1$.

2.3. Scintillation Line Shape.   The shape of the scintillation line (i.e., the response of the detector to the monoenergetic source uniformly distributed over the detector's volume) is another sensitive component of the analysis. A common approximation with a normal distribution is failing to describe the tails of the MC-generated monoenergetic response already at the statistics of the order of 10^3 events. This was notified already in the first phase of Borexino and the approximation of the scintillation line shape with generalized gamma function [29]

have been used to fit monoenergetic ^{210}Po peak in the solar ^{7}Be neutrino analysis [7, 30, 31]. The generalized gamma function (GGC) was developed for the energy estimator based on the total collected charge, but it provided a reasonable approximation for the energy estimator based on the number of triggered PMTs given the moderate statistics corresponding to the total amount of the events in ^{210}Po peak. The fit quality of the ^{210}Po peak is rather insensitive to the residual deviations in the tails. This is not the case for the precise ^{14}C spectrum modeling, as all the events in the fraction of the ^{14}C spectrum above the energy threshold originate from the spectral smearing. An ideal detector's response to the point-like monoenergetic source at the center is a perfect binomial distribution and it would be well approximated by the Poisson distribution. When dealing with a real response one should adjust the "base distribution" width to take into account at least the additional smearing of the signal due to various factors. The problem with binomial "base function" (or with its Poisson approximation) is that its width is defined by the mean value. In case of Poisson the variance of the signal coincides with mean μ. A better approximation of the response function was tested with MC model, namely, the scaled Poisson (SP) distribution:

$$f(x) = \frac{\mu^{xs}}{(xs)!}\, e^{-\mu}, \tag{2}$$

featuring two parameters that could be evaluated using expected mean and variance of the response:

$$s = \frac{\sigma_n^2}{n} \text{ and } \mu = \frac{n^2}{\sigma_n^2}. \tag{3}$$

The agreement of the approximation and the detector response function was tested with Borexino MC model and it was found that at low energies (2) better reproduces the scintillation line shape compared to the generalized gamma function up to the statistics of 10^8, while at energies just above the ^{14}C tail both distributions give comparable approximation. The quality of the fit was estimated using χ^2 criterion, for example, with 10^7 total statistics (these events are uniformly distributed in the detector and then the FV is selected) for $n = 50$ (approximately 140 keV) we found $\chi^2/\text{n.d.f.} = 88.0/61$ for the GGC compared to $\chi^2/\text{n.d.f.} = 59.3/61$ for the SP distribution.

As proven by MC tests, the SP distribution as a base function works well in the energy region of interest despite of the additional smearing due to the factors enlisted in the previous paragraph. This is a result of the "absorption" of the relatively narrow nonstatistical distributions by the much wider base function; as follows from MC, such an absorption results in the smearing of the total distribution without changing its shape.

As was noted above, the fit was performed in n scale. All the theoretical spectra involved in the fit were first translated into the n scale and then smeared

using resolution function (2) with μ and scale factor s calculated using (3). As is clear from the discussion above, the detector's response has the shape described by (2) only in the "natural" n scale. If the measured values of n were converted into the energy, the shape would be deformed because of the nonlinearity of the energy estimator scale with respect to the energy, complicating the construction of the precise energy response.

2.4. Standard Fit. The "standard" options of the spectral fit are: number of triggered PMTs in a fixed time window of 230 ns (npmts) used as energy estimator; 62–220 npmts fit range; (75.5 ± 1.5) t fiducial volume (defined by the condition $R < 3.02$ m and $|Z| < 1.67$ m).

The rate of the solar neutrinos is constrained either at the value found by Borexino in the different energy range $(R(^7\mathrm{Be}) = (48 \pm 2.3)$ cpd [7]) or fixed at the prediction of the SSM in the SMW/LMA oscillation scenario $(R(pep) = 2.80$ cpd, $R(\mathrm{CNO}) = 5.36$ cpd). All counts here and below are quoted for 100 t of LS.

The $^{14}\mathrm{C}$ rate was constrained at the value found in independent measurement with the second cluster $R(^{14}\mathrm{C}) = (40 \pm 1)$ Bq (or $R(^{14}\mathrm{C}) = (3.456 \pm 0.0864) \cdot 10^6$ cpd). The synthetic pile-up rate was constrained at the values found with the algorithm. The normalization factors for other background components were mainly left free ($^{85}\mathrm{Kr}$, $^{210}\mathrm{Bi}$, and $^{210}\mathrm{Po}$) and the fixed rate of $^{214}\mathrm{Pb}$ ($R(^{214}\mathrm{Pb}) = 0.06$ cpd) was calculated on the base of the amount of identified radon events. The light yield and two energy resolution parameters (v_T and σ_{int}) are left free. The position of $^{210}\mathrm{Po}$ is also left free in the analysis, decoupling it from the energy scale.

2.5. Systematics Study. An evident source of systematics is the uncertainty of the FV. The FV mass is defined using position reconstruction code, residual bias in the reconstructed position is possible. The systematic error of the position reconstruction code was defined during the calibration campaign, comparing the reconstructed source position with the nominal one [27, 28]. At the energies of interest the systematic error on the FV mass is 2%.

The stability and robustness of the measured pp-neutrino interaction rate was verified by performing fits varying initial conditions, including fit energy range, method of pile-up construction, and energy estimator. The distribution of the central values for pp-neutrino interaction rates obtained for all these fit conditions was then used as an estimate of the maximal systematic error (partial correlations between different factors are not excluded).

The remaining external background in the fiducial volume at energies relevant for the pp-neutrino study is negligible. In the particular case of the very low-energy part of the spectrum, the fit was repeated in five smaller fiducial volumes (with smaller radial and/or z-cut), which yields very similar results, indicating the absence of the influence of the external backgrounds at low energies.

3. RESULTS AND IMPLICATIONS

The solar pp-neutrino interaction rate measured by Borexino is $pp = (144 \pm 13(\text{stat.}) \pm 10(\text{syst.})$ cpd/100 t, compatible with the expected rate of $pp_{\text{theor}} = (131 \pm 2)$ cpd/100 t. The corresponding total solar pp-neutrino flux is $\phi_{pp}(\text{Borex}) = (6.6 \pm 0.7) \cdot 10^{10}$ cm$^{-2} \cdot$s^{-1}, in a good agreement with the combined best fit value of the radiochemical and other solar experiments $\phi_{pp}(\text{other}) = (6.0 \pm 0.8) \cdot 10^{10}$ cm$^{-2} \cdot$s^{-1} [11]. Both are in agreement with the expected value of $6.0 \cdot (1.000 \pm 0.006) \cdot 10^{10}$ cm$^{-2} \cdot$s^{-1}.

The survival probability for electron neutrino from pp-reaction is $P_{ee}(\text{Borex}) = 0.64 \pm 0.12$. This is the fourth energy range explored by Borexino, all the Borexino results on the electron neutrino survival probability are presented graphically in Fig. 3.

Taking into account that measurements of Borexino and other experiments are independent, the results can be combined:

$$\phi_{pp} = (6.37 \pm 0.46) \cdot 10^{10} \text{ cm}^{-2} \cdot \text{s}^{-1}.$$

The electron neutrino survival probability measured in all solar but Borexino experiment is $P_{ee}(\text{other}) = 0.56 \pm 0.08$, combining it with Borexino one, we obtain

$$P_{ee} = 0.60 \pm 0.07,$$

well compatible with theoretical prediction of the MSW/LMA model $0.561^{+0.030}_{-0.042}$.

All available measurements of the solar neutrino fluxes are shown in Table 2. The total energy production in the solar reactions observed till now (by detecting corresponding neutrino fluxes) is (4.04 ± 0.28) W $\cdot$ s^{-1} in a good agreement with a
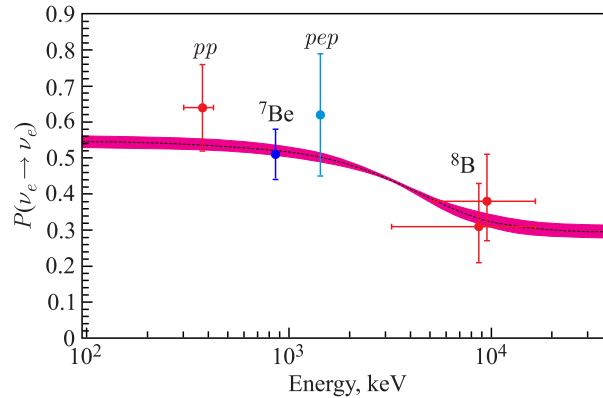
Fig. 3. Survival probabilities for electron neutrino (Borexino only data from [7,27,32,33])

Table 2. **The Standard Solar Model predictions (for high metallicity and low metallicity abundances) and current experimental status of the solar neutrino flux measurement. The limits are given for 90% C.L. The corresponding energy release is calculated in the last column**

Reaction	GS98 [34]	AGS09 [35]	Units $cm^{-2} \cdot s^{-1}$	Measurement	MeV/1ν	L, 10^{26} $W \cdot s^{-1}$
pp	5.98 ± 0.04	6.03 ± 0.04	$\times 10^{10}$	6.0 ± 0.8 [11] 6.6 ± 0.7 [26] 6.37 ± 0.46	13.10	3.76 ± 0.28
pep	1.44 ± 0.012	1.47 ± 0.012	$\times 10^{8}$	1.6 ± 0.3 [33]	11.92	0.009 ± 0.002
^{7}Be	5.00 ± 0.07	4.56 ± 0.07	$\times 10^{9}$	4.87 ± 0.24 [7]	12.60	0.276 ± 0.014
^{8}B	5.58 ± 0.14	4.59 ± 0.14	$\times 10^{6}$	5.25 ± 0.16 [36]	6.63	$1.57 \pm 0.05 \cdot 10^{-4}$
hep	8.0 ± 2.4	8.3 ± 2.5	$\times 10^{3}$	< 23 [37]		
^{13}N	2.96 ± 0.14	2.17 ± 0.14	$\times 10^{8}$	CNO:		
^{15}O	2.23 ± 0.15	1.56 ± 0.15	$\times 10^{8}$	< 7.4 [33]		
^{17}F	5.52 ± 0.17	3.40 ± 0.16	$\times 10^{6}$			

total measured $L_\odot = 3.846 \cdot 10^{26}$ W $\cdot$ s^{-1}. There is not much space left for the unknown energy sources, the 90% C.L. lower limit for the total energy production (conservatively assuming zero contribution from the not-observed reactions) is $L_{\text{tot}} = 3.68 \cdot 10^{26}$ W $\cdot$ s^{-1}. If one assumes that such an unknown source exists, its total power with 90% probability cannot exceed $0.15 \cdot 10^{26}$ W $\cdot$ s^{-1}. In other words, no more than 4% of the total energy production in the Sun is left for the unknown energy sources, confirming that the Sun shines due to the thermonuclear fusion reactions.

REFERENCES

1. *Chapman G. A.* Solar Luminosity // Encyclopedia of Planetary Science, Encyclopedia of Earth Science. Springer, Netherlands, 1997. P. 748–748.

2. *Fröhlich C., Lean J.* The Sun's Total Irradiance: Cycles, Trends and Related Climate Change Uncertainties since 1976 // Geophys. Res. Lett. 1998. V. 25, No. 23. P. 4377–4380.

3. *Bahcall J. N.* Neutrino Astrophysics. Cambridge Univ. Press, 1989.

4. *Bahcall J. N.* The Luminosity Constraint on Solar Neutrino Fluxes // Phys. Rev. C. 2002. V. 65. P. 025801.

5. *Foukal P. et al.* Variations in Solar Luminosity and Their Effect on the Earth's Climate // Nature. 2006. V. 443. P. 161–166.

6. *Fiorentini G., Ricci B.* How Long Does It Take for Heat to Flow through the Sun? // Comments on Astrophys. 1999. V. 1. P. 49–51.

7. *Bellini G. et al.* Precision Measurement of the ^{7}Be Solar Neutrino Interaction Rate in Borexino // Phys. Rev. Lett. 2011. V. 107, No. 14. P. 141302.

8. *Calabresu E., Fiorentini G., Lissia M.* Physics Potentials of pp and pep Solar Neutrino Fluxes // Astropart. Phys. 1996. V. 5, No. 2. P. 205–214.

9. *Bahcall J. N.* Why Do Solar Neutrino Experiments below 1 MeV? hep-ex/0106086.

10. *Raghavan R. S.* Discovery Potential of Low Energy Solar Neutrino Experiments. Notes for APS-SAWG. 2004.

11. *Abdurashitov J. N. et al.* Measurement of the Solar Neutrino Capture Rate with Gallium Metal. III. Results for the 2002–2007 Data-Taking Period // Phys. Rev. C. 2009. V. 80. P. 015807.

12. *Kaether F. et al.* Reanalysis of the Gallex Solar Neutrino Flux and Source Experiments // Phys. Lett. B. 2010. V. 685, No. 1. P. 47–54.

13. *Grieb C., Link J. M., Raghavan R. S.* Probing Active to Sterile Neutrino Oscillations in the Lens Detector // Phys. Rev. D. 2007. V. 75. P. 093006.

14. *Raghavan R. S. pp* Solar Neutrino Spectroscopy. Return of the Indium Detector // Phys. Rev. Lett. 2001.

15. *Klapdor-Kleingrothaus H. V.* {GENIUS} — A New Facility of Non-Accelerator Particle Physics // Nucl. Phys. B. Proc. Suppl. 2001. V. 100, No. 13. P. 350–355.

16. *Huang Y. H. et al.* Potential for Precision Measurement of Solar Neutrino Luminosity by {HERON} // Astropart. Phys. 2008. V. 30, No. 1. P. 1–11.

17. *Adams J. S. et al.* The HERON Project. Ch. 8 // Low Energy Solar Neutrino Detection. 2002. P. 70–80.

18. *Kawasaki K. et al.* XMASS(XENON) II. Ch. 10 // Ibid. P. 91–97.

19. *McKinsey D. N.* CLEAN: A Self-Shielding Detector for Characterizing the Low Energy Solar Neutrino Spectrum. Ch. 12 // Ibid. P. 106–115.

20. *Sarrat A.* HELLAZ: A Low Energy Neutrino Spectrometer // Nucl. Phys. Proc. Suppl. 2001. V. 95. P. 177–180.

21. *Ejiri H.* MOON (Mo Observatory Of Neutrinos) for Low Energy Neutrinos. Ch. 4 // Low Energy Solar Neutrino Detection. 2002. P. 29–36.

22. *Broggini C.* MuNu as a Solar Neutrino Detector. Ch. 14 // Ibid. P. 132–141.

23. *McKinsey D. N., Doyle J. M.* Liquid Helium and Liquid Neon-Sensitive, Low Background Scintillation Media for the Detection of Low-Energy Neutrinos // J. Low Temp. Phys. 2000. V. 118, No. 3–4. P. 153–165.

24. *Smirnov O. Yu., Zaimidoroga O. A., Derbin A. V.* Search for Solar *pp*-Neutrinos with an Upgrade of CTF Detector // Phys. Atom. Nucl. 2003. V. 66, No. 4. P. 712–723.

25. *Derbin A. V., Smirnov O. Yu., Zaimidoroga O. A.* On the Possibility of Detecting Solar *pp*-Neutrino with the Large-Volume Liquid Organic Scintillator Detector // Phys. Atom. Nucl. 2004. V. 67, No. 11. P. 2066–2072.

26. *Bellini G. et al.* Final Results of Borexino Phase-I on Low-Energy Solar Neutrino Spectroscopy // Phys. Rev. D. 2014. V. 89. P. 112007.

27. *Bellini G. et al.* Neutrinos from the Primary Proton–Proton Fusion Process in the Sun // Nature. 2014. V. 512. P. 383–386.

28. *Back H. et al.* Borexino Calibrations: Hardware, Methods, and Results // J. Instr. 2012. V. 7, No. 10. P. P10018.

29. *Smirnov O. Yu.* An Approximation of the Ideal Scintillation Detector Line Shape with a Generalized Gamma Distribution // Nucl. Instr. Meth. A. 2008. V. 595, No. 2. P. 410–418.

30. *Arpesella C. et al.* First Real Time Detection of ^{7}Be Solar Neutrinos by Borexino // Phys. Lett. B. 2008. V. 658. P. 101–108.

31. *Arpesella C. et al.* Direct Measurement of the ^{7}Be Solar Neutrino Flux with 192 Days of Borexino Data // Phys. Rev. Lett. 2008. V. 101, No. 9. P. 091302.

32. *Bellini G. et al.* Measurement of the Solar ^{8}B Neutrino Rate with a Liquid Scintillator Target and 3 MeV Energy Threshold in the Borexino Detector // Phys. Rev. D. 2010. V. 82. P. 033006.

33. *Bellini G. et al.* First Evidence of *pep* Solar Neutrinos by Direct Detection in Borexino // Phys. Rev. Lett. 2012. V. 108. P. 051302.

34. *Grevesse N., Sauval A. J.* Standard Solar Composition // Space Sci. Rev. 1998. V. 85, No. 1–2. P. 161–174.

35. *Asplund M. et al.* The Chemical Composition of the Sun // Ann. Rev. Astron. Astrophys. 2009. V. 47, No. 1. P. 481–522.

36. *Aharmim B. et al.* Low-Energy-Threshold Analysis of the Phase I and Phase II Data Sets of the Sudbury Neutrino Observatory // Phys. Rev. C. 2010. V. 81. P. 055504.

37. *Aharmim B. et al.* A Search for Neutrinos from the Solar *hep* Reaction and the Diffuse Supernova Neutrino Background with the Sudbury Neutrino Observatory // Astrophys. J. 2006. V. 653, No. 2. P. 1545.